Crystallization of block copolymers: 3. Crystallization behaviour of an ε-caprolactone–butadiene diblock copolymer

Shuichi Nojima*, Haruo Nakano, Yoshikazu Takahashi and Tamaichi Ashida

Department of Biotechnology, School of Engineering, Nagoya University, Nagoya 464-01, Japan

(Received 29 October 1993; revised 10 January 1994)

The crystallization behaviour of an ε-caprolactone-*block*-butadiene diblock copolymer was observed by small-angle X-ray scattering employing synchrotron radiation. The processes of primary and secondary crystallizations were separately analysed by procedures usually used for homopolymer crystallization, and were compared with the case of a poly(ε-caprolactone) homopolymer (PCL). The Avrami analysis at the primary crystallization showed an exponent n ranging from 2 to 3. This value is comparable to n evaluated for PCL and also n widely reported for crystalline homopolymers, indicating that the crystallization of the PCL block drives the primary stage without the influence of the existing microphase structure of the block copolymer. In the secondary crystallization, on the other hand, the rate was significantly retarded when a microphase structure existed in the system.

(Keywords: diblock copolymer; microphase structure; crystallization)

INTRODUCTION

The crystallization process of homopolymers is mainly divided into three stages: primary crystallization, secondary crystallization and crystal perfection[1,2]. In the primary crystallization, nucleation takes place to develop into the spherulitic morphology. The crystallization rate at this stage is successfully described by the Avrami equation. The secondary crystallization involves further crystallization of molten polymer within the spherulites after the primary crystallization. The general observation at this stage is a distinct drop in the Avrami exponent n. The crystal perfection is the final step in the crystallization and including lamellar thickening of poorly crystallized polymers.

The crystallization of block copolymers starts from a microphase structure (sphere, cylinder or lamella) when they are cast from a good solvent or quenched from high temperature. Therefore, the existing microphase structure will affect the crystallization behaviour to give a characteristic morphology[3–16]. There are, however, few experimental studies of the crystallization behaviour of block copolymers, particularly those that take the microphase structure into account.

In our recent studies[17,18], we examined the crystallization behaviour of a crystalline–amorphous diblock copolymer, ε-caprolactone-*block*-butadiene (PCL-*b*-PB), by small-angle X-ray scattering employing synchrotron radiation (SR-SAXS). The phase transformation of PCL-*b*-PB was interesting because the microphase structure was completely destroyed by the subsequent crystallization of the PCL block. Additionally, the crystallization mode of PCL-*b*-PB at the primary stage was found to be similar to that of a poly(ε-caprolactone) homopolymer (PCL), while the secondary crystallization was significantly different between PCL-*b*-PB and PCL.

In this study, we quantitatively analyse the primary and secondary crystallizations of PCL-*b*-PB observed by SR-SAXS. The Avrami equation, which reflects the nucleation mechanism and growth mode, was used for the analysis of the primary crystallization. The secondary crystallization was treated by a phenomenological equation widely used for further crystallization within the spherulites. These analyses will elucidate the similarity and dissimilarity of the crystallization behaviour between homopolymers and block copolymers. From the results of the analyses, the crystallization mechanism of microphase-separated block copolymers will be discussed.

EXPERIMENTAL

Materials

The ε-caprolactone–butadiene diblock copolymers were synthesized by successive anionic polymerizations under vacuum[17]. The butadiene monomer in toluene was first polymerized at room temperature over two days with n-butyllithium as the initiator, then ε-caprolactone monomer was added to synthesize the block copolymer at −10°C to −15°C over 5–15 min. The butadiene monomer/initiator ratio and the reaction time of the ε-caprolactone monomer were adjusted to obtain copolymers with various compositions and molecular weights. We also took care to prevent depolymerization (backbiting) by the living ε-caprolactone end during the anionic growth of the PCL block[19]. The samples

* To whom correspondence should be addressed at present address: Department of Materials Science, Japan Advanced Institute of Science and Technology (JAIST), Tatsunokuchi, Ishikawa 923-12, Japan

0032-3861/94/16/3479–08

Table 1 Characterization of the polymers used in this study

Notation	Polymer	Total M_w[a]	M_w/M_n[a]	PCL/PB ratio[b] (vol%)	Microstructure of the PB chain[b] (%)			T_m[c] (°C)
					cis-1,4	*trans*-1,4	1,2-linkage	
B4	PCL-*b*-PB	13 700	1.19	14:86	36	52	12	~41
B5	PCL-*b*-PB	9 400	1.05	27:73	37	53	10	~41
B6	PCL-*b*-PB	12 500	1.35	35:65	36	53	11	~43
B7	PCL-*b*-PB	12 400	1.10	61:39	36	52	12	~55
B11	PCL-*b*-PB	14 100	1.09	26:74	35	51	14	~45
PCL2	PCL	8 200	1.65					54.3

[a] Determined by g.p.c.
[b] Determined by ^{1}H n.m.r.
[c] Determined by d.s.c.

thus synthesized were characterized by gel permeation chromatography (g.p.c), and the PCL content was evaluated by ^{1}H n.m.r. (Varian GEMINI-200)[20]. The melting temperature of the PCL block was measured by differential scanning calorimetry (d.s.c.) (MAC Science model 3100) at a heating rate of 5°C min^{-1}.

Table 1 shows the molecular characterization results. The following specific volumes were used to calculate the volume fraction of each block in the copolymer. For polybutadiene[21]

$$v_{sp} = 1.1138 + (8.24 \times 10^{-4})T \quad (1)$$

and for poly(ε-caprolactone)[22]

$$v_{sp} = 0.9106 + (6.013 \times 10^{-4})T \quad (2)$$

where v_{sp} is in cm^3 g^{-1} and T is in °C. All the copolymers except B7 showed a diffuse melting endotherm with a melting temperature T_m around 42°C. B7 had a sharp endothermic peak at ca. 55°C, which was similar in shape to the case of PCL2. B4 has a microphase separation temperature T_s probably below room temperature, B5 and B6 have T_s around T_m and B7 and B11 have T_s far above T_m judging from the SAXS curve above T_m. Therefore, B5 and B6, which are homogeneous at temperatures above T_m, present a microphase structure just after quenching, while B7 and B11 show a microphase structure even at temperatures above T_m. Consequently, a cooperative morphology formation between microphase separation and crystallization is expected for B5, B6, B7 and B11, while only crystallization occurs for B4.

The microphase structure of B7 and B11 can be deduced from the SAXS curve at a temperature above T_m and the PCL content in the copolymer[23]. The SAXS curve for B7 has two definite diffractions and their angular positions correspond to a ratio of 1:2. Therefore, B7 takes a lamellar microphase structure before crystallization. B11 has a few diffractions and the angular positions definitely correspond to a ratio of $1:\sqrt{3}:2$, suggesting a spherical structure with the PCL block inside.

Time-resolved SAXS measurement with synchrotron radiation[24,25]

The crystallization behaviour was examined by SAXS with synchrotron radiation. The experiments were carried out at the National Laboratory for High Energy Physics, Tsukuba, Japan (Photon Factory) with the small-angle X-ray equipment for solutions (SAXES) installed on beamline BL-10C[26,27]. The storage ring was operated at an energy level of 2.5 GeV with a ring current of 250–300 mA over a period of 12 or 24 h. The SAXES employs point-focusing optics with a double-flat monochromator followed by a bent cylindrical mirror. The incident beam intensity (with $\lambda = 0.1488$ nm) was monitored by an ionization chamber to correct for a minor decrease in the intensity during the measurements. The scattered intensity was detected by a position-sensitive proportional counter (PSPC) with 512 channels, and the distance between the sample and the PSPC was about 2000 mm. The geometry was further checked with chicken tendon collagen, which gives a set of sharp diffractions corresponding to 65.3 nm. Details of the optics and instrumentation are described elsewhere[27].

The sample temperature was controlled by circulating water with a constant temperature[17,28], by which temperature fluctuations were kept to within ±0.2°C throughout the experiment. The crystallization was started by dropping the water temperature from ca. 60°C (homogeneous for B4, B5, B6 and PCL2 and microphase separated for B7 and B11) to T_c and it took about 1 min for the sample to reach T_c. The SAXS intensity was collected as an accumulation of the scattered intensity during 10 or 20 s from the beginning of the temperature drop, and the measurement was continued until the overall scattering profile had changed no more.

The SAXS intensity measured was corrected for the decrease in the ring current and background scattering. Since the optics of the SAXES is point focusing, the scattered intensity was not corrected for the smearing effect from the finite cross-section of the primary beam[27]. The SAXS curve against s ($=2\sin\theta/\lambda$, where 2θ is the scattering angle) was obtained as a function of time t after the temperature had dropped to T_c.

Analysis of time-resolved SAXS curves

Primary crystallization. The primary crystallization was analysed by the Avrami equation[29–31], which is widely used for the analysis of homopolymer crystallization. The volume fraction $X(t)$ of the crystal at time t is given by

$$X(t) = 1 - \exp[-(Kt)^n] \quad (3)$$

where K is a rate constant and n is the Avrami exponent expressing the mode of crystallization. $X(t)$ is normalized so as to take unity at $t = \infty$. The volume change evaluated from a dilatometric measurement or an exothermic heat flow measured by d.s.c. is usually used for $X(t)$. The scattering power[32] $Q(t)$ or intensity maximum[26,28] $I_{max}(t)$

at time t from the crystalline morphology (or two-phase system) was also used for the analysis of the SR-SAXS curves assuming that the alternating structure (and also the degree of crystallinity) within the crystalline morphology does not change during the primary crystallization[33]. After normalizing $I_{max}(t)$ by the final intensity $I_{max}(\infty)$, we obtain

$$X(t) = I_{max}(t)/I_{max}(\infty) \quad (4)$$

Then the Avrami equation is reduced to

$$\log\{-\ln[1 - I_{max}(t)/I_{max}(\infty)]\} = n(\log t + \log K) \quad (5)$$

Generally speaking, the scattered intensity (or volume fraction of the crystalline morphology) is small at the primary crystallization and is difficult to extract from a comparable background scattering. It is therefore hard to evaluate n with an acceptable accuracy[1,2]. This is the most ambiguous point in the Avrami analysis because the evaluation of n involves the double logarithm of $X(t)$. If the diffracted intensity $I'_{max}(t)$ from the microphase structure can be used as $X(t)$, then the analysis will be more reliable because $I'_{max}(t)$ is strong enough at the early stage of crystallization. In an earlier paper[17], we found that the phase transformation occurred directly from the microphase structure into the crystalline morphology and no third phase appeared. That is, the system during the phase transformation is a mosaic structure consisting of the microphase structure and crystalline morphology for all t, and we can state

$$X(t) = 1 - I'_{max}(t)/I'_{max}(0) \quad (6)$$

where $I'_{max}(0)$ is the diffracted intensity just before crystallization. Inserting equation (6) into equation (3) we obtain

$$\log\{-\ln[I'_{max}(t)/I'_{max}(0)]\} = n(\log t + \log K) \quad (7)$$

It is therefore possible to evaluate n from the plot of $\log\{-\ln[I'_{max}(t)/I'_{max}(0)]\}$ against $\log t$.

Secondary crystallization. Secondary crystallization means further crystallization of molten polymers within the spherulites after the primary crystallization. Hillier[34] gave the expression for the secondary crystallization as

$$X(t) = 1 - \exp[-K'(t - \tau)] \quad (8)$$

where K' is the rate constant for this stage and τ is the time at which the secondary crystallization starts. Equation (8) has been applied for many homopolymers and found to describe adequately the secondary crystallization[34-37]. Here, we use equation (8) phenomenologically for the crystallization process of the present block copolymers after the primary stage ($0.6 < I_{max}(t)/I_{max}(\infty) < 0.95$). It is possible to evaluate K' and τ by plotting $\ln[1 - X(t)]$ against t with $X(t)$ given by equation (4).

Next, we consider the dimensionless parameter θ defined by

$$\theta = K'/K \quad (9)$$

Here, θ represents the ratio of the rate constants for the primary and secondary crystallizations and depends on the crystallization behaviour and T_c. For example, θ becomes smaller when the secondary crystallization proceeds more slowly with the same crystallization rate at the primary stage. Therefore, θ gives quantitative information about the relative rates of the primary and secondary crystallizations when the crystallization processes are compared among different polymers or different conditions.

RESULTS

Time-resolved SAXS curves

In an earlier paper[17], we showed that the crystallization behaviour of PCL-*b*-PB was unique because of the intervention of a microphase structure. *Figure 1* shows time-sliced SAXS curves plotted against s ($=2\sin\theta/\lambda$) for three typical cases with different T_s, where each SAXS curve is symmetrical about $s=0$.

B4 has a T_s lower than room temperature, so that no sign of microphase separation has appeared during crystallization (*Figure 1a*). That is, in addition to the diffuse scattering arising from the correlation hole effect of the block copolymer (0 s), a strong scattering appears from the crystalline morphology at a lower angle (indicated by arrows) after quenching (140 s), probably the peak located inside the beam stop. The strong scattered intensity grows with time and the diffuse scattering decreases and finally disappears (1480 s). B5 (and also B6) has a T_s around T_m, so that the microphase separation occurs simultaneously with crystallization. In *Figure 1b*, the diffuse-scattering maximum is completely replaced by a sharp diffraction just after quenching (65 s), and at $t=220$ s a second intensity maximum appears at a smaller angle (indicated by arrows). This maximum grows with time and the sharp diffraction reduces in intensity and finally disappears (1060 s). That is, the regular microphase structure formed just after quenching, with a characteristic length (D) of 10.3 nm, is steadily replaced by the crystalline morphology with a long spacing (L) of 19.1 nm. For B11 (and also B7), the copolymer has already a microphase structure (lamellar structure for B7 and spherical structure for B11) at 60°C ($> T_m$), and crystallization of the PCL block starts from this structure. In *Figure 1c*, the SAXS curve just after quenching is similar in shape to that at 60°C ($D=13.5$ nm), and at $t=110$ s another scattering maximum (indicated by arrows) appears at a lower angle ($L=23.1$ nm). This second maximum grows with time and the diffracted intensity gradually decreases, although a shoulder remains at the angular position of the diffraction (815 s). A conventional SAXS measurement revealed that the shoulder finally disappeared at large t.

Overall features of the crystallization

Figure 2 shows the time dependence of the normalized intensity maximum $I_{max}(t)/I_{max}(\infty)$, the peak intensity divided by the final intensity arising from the crystalline morphology, for B6 crystallized at $T_c = 23.5$°C, 25.0°C, 26.5°C, 28.0°C and 30.5°C. *Figure 2* shows the growth features of the crystalline morphology in the system at each T_c. The growing rate is slower with increasing T_c, which is qualitatively similar to an earlier result with a compatible blend of PCL and polystyrene oligomer (PCL/PSO)[28]. Although the t dependence of the intensity maximum shows different curves in PCL/PSO, they coincide with each other and make one master curve when $I_{max}(t)/I_{max}(\infty)$ is plotted against the reduced time $t/t_{1/2}$, where $t_{1/2}$ is the crystallization half-time. This means that the overall features of the morphology formation are the same as those of PCL, and the crystallization of PCL controls the whole rate of morphology formation in PCL/PSO.

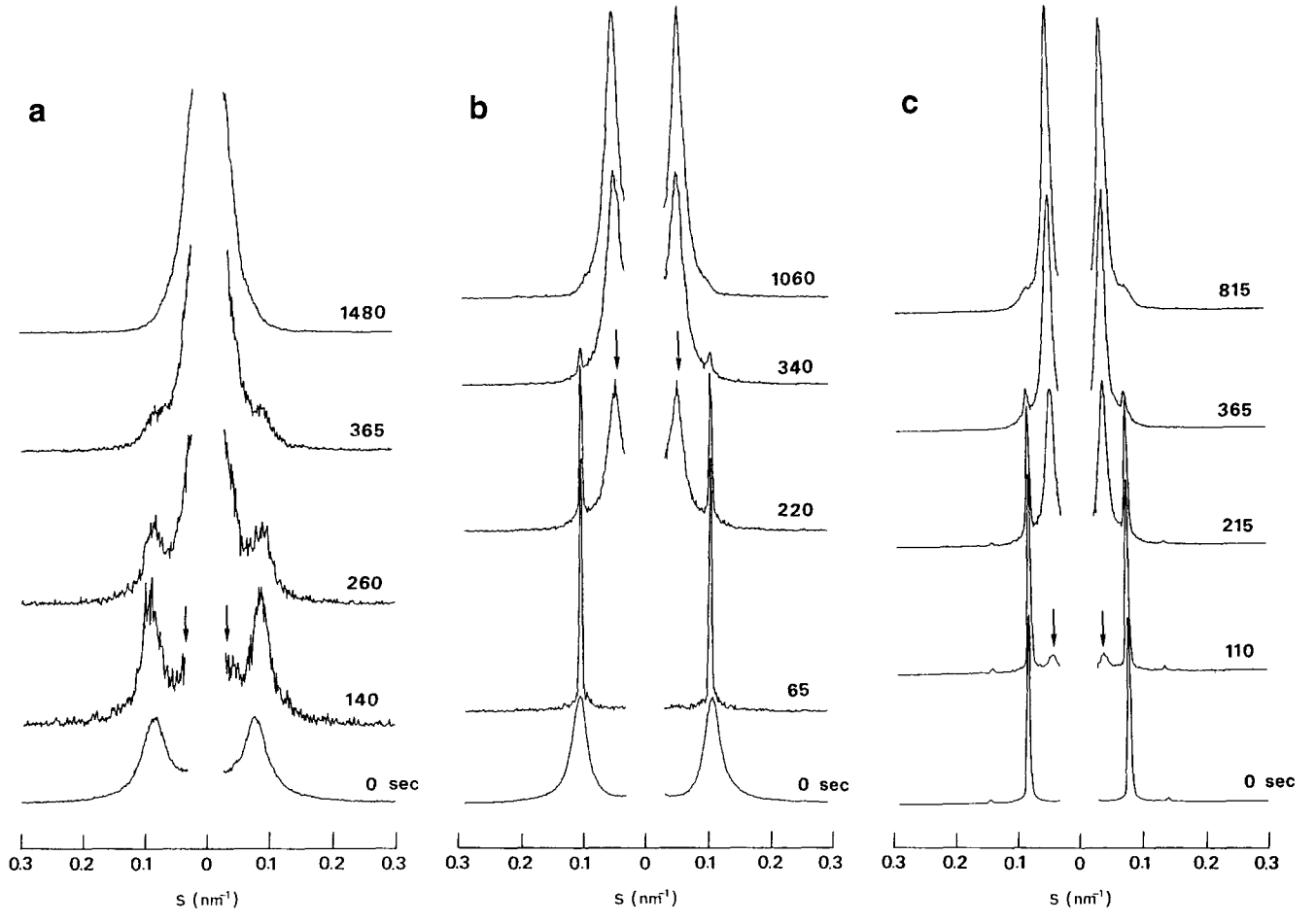

Figure 1 Time-resolved SAXS curves plotted against wavenumber s ($=2\sin\theta/\lambda$) for (a) B4 quenched from 60°C to 17.5°C, (b) B5 quenched from 60°C to 27.0°C and (c) B11 quenched from 60°C to 27.0°C. The number on each curve represents the time elapsed since the sample was quenched. The SAXS curve for 0 s is the result of an accumulation period of 300 s at 60°C and has been converted to a 10 s accumulation, while the other curves are from 10 s accumulations

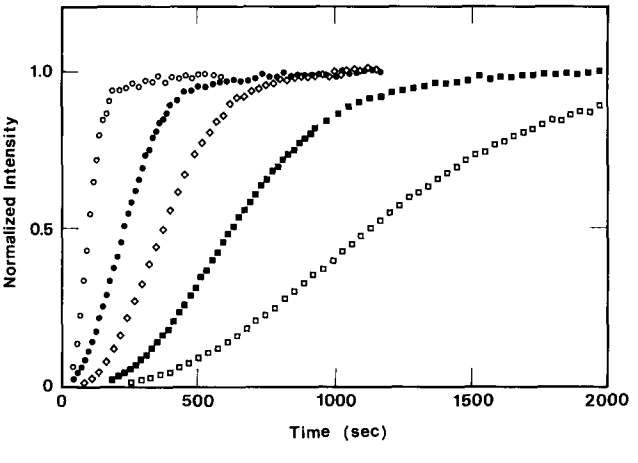

Figure 2 Normalized intensity maximum plotted against crystallization time for B6 crystallized at 23.5°C (○), 25.0°C (●), 26.5°C (◇), 28.0°C (■) and 30.5°C (□)

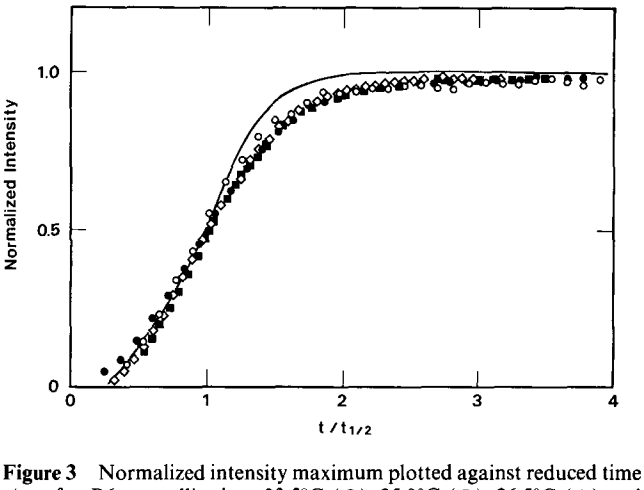

Figure 3 Normalized intensity maximum plotted against reduced time $t/t_{1/2}$ for B6 crystallized at 23.5°C (○), 25.0°C (●), 26.5°C (◇) and 28.0°C (■). Some data points are omitted for clarity. The solid curve represents the results for the PCL homopolymer

Figure 3 shows the plots of $I_{max}(t)/I_{max}(\infty)$ against $t/t_{1/2}$ for B6, and the different curves make one master curve, suggesting that the crystallization behaviour is the same irrespective of T_c. The solid curve in *Figure 3* represents the results for PCL and PCL/PSO, where the crystallization of PCL controls the morphology formation. The data points agree well with the solid curve until $t/t_{1/2}$ reaches 1. The master curve at $t/t_{1/2}>1$ is, on the other hand, significantly different from the solid curve: the copolymer crystallization is retarded in comparison to the PCL crystallization. In particular, the normalized intensity for PCL-*b*-PB gradually increases at $t/t_{1/2}>2$ towards the completion of crystallization. *Figure 3* indicates that the crystallization behaviour of PCL-*b*-PB

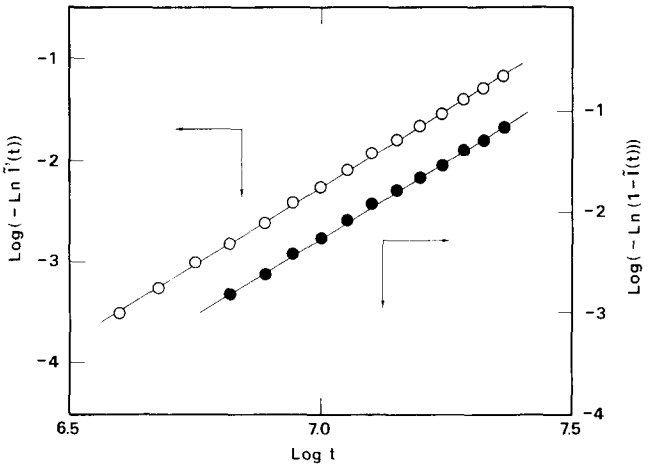

Figure 4 The Avrami plots calculated from the scattered intensity maximum (●) and the diffracted intensity maximum (○) for B11 crystallized at 32.3°C ($\tilde{I}'(t)=I'_{max}(t)/I'_{max}(0)$ and $\tilde{I}(t)=I_{max}(t)/I_{max}(\infty)$)

Table 2 Avrami exponents evaluated from diffracted intensity (n_1) and scattered intensity (n_2)

Sample	T_c (°C)	n_1	n_2
B4	17.5–24.9		2.8–3.0
B5	25.0–31.5	2.7–2.9	2.2–3.1
B6	23.5–30.5	2.3–2.7	2.6–2.8
B7	34.5–40.4	2.4–2.8	2.0–2.6
B11	27.0–32.3	2.7–2.9	2.3–3.2
PCL2	30.8–39.7		2.2–2.9
HDPE[a]	120–126		1.9–3.2
PEO[b]	35–58		2.0–3.1

[a] From ref. 38
[b] From ref. 39

is not the same as that of PCL at the secondary crystallization, and some effect arising from the constituent block copolymer (for example, a remaining microphase structure or covalently bonded amorphous block) prominently appears.

Analysis of the primary crystallization

Figure 4 shows examples of Avrami plots obtained from the t dependences of the scattered intensity (equation (5)) and diffracted intensity (equation (7)) for B11 at $T_c=32.3$°C. Here, the data from the first 25% in intensity were used because the Avrami analysis is valid only for the early stage of crystallization. Both lines in *Figure 4* have almost the same slope and n is easily evaluated. We were able to obtain similar plots for all the samples at each T_c, although some plots did not have enough data points to determine n unambiguously because of the fast phase transformation. The plot obtained from the diffracted intensity has more data points than that from the scattered intensity at the beginning of crystallization, and seems to make the Avrami analysis more reliable.

The Avrami exponents thus evaluated are summarized in *Table 2* for B4, B5, B6, B7, B11 and PCL2. The value of n evaluated for PCL-*b*-PB ranges from 2 to 3 irrespective of the PCL content. These values listed in *Table 2* are indistinguishable from n evaluated for PCL2 and also n widely reported for typical crystalline homopolymers. For example, n ranging from 2 to 3 is reported for a high density polyethylene (HDPE)[38], poly(ethylene oxide) (PEO)[39] and a compatible blend of poly(ε-caprolactone) and poly(vinyl chloride)[26,40]. In these studies, the crystallization process was assigned as two-dimensional with a heterogeneous nucleation on the basis of the Avrami analysis and spherulite observations. This agreement of n suggests that the nucleation mode is the same for PCL-*b*-PB and general crystalline homopolymers. That is, the primary stage of phase transformation for PCL-*b*-PB is driven by the crystallization of the PCL block, and whatever the initially existing microphase structure, it does not affect the primary crystallization.

At the end of the primary stage of crystallization, we observed a spherulitic morphology by optical microscopy. The spherulites were extremely open in texture compared with those of pure PCL, and a regular extinction band, sometimes observed in binary blends including PCL[41–43], was not observed. These facts suggest that PCL-*b*-PB first forms poorly crystallized spherulites, and further crystallization will occur extensively within the spherulites at the secondary stage.

Analysis of the secondary crystallization

The secondary crystallization was quantitatively analysed using equations (8) and (9). The effective range of this stage is rather arbitrary, but it is generally said that equation (8) is useful for times larger than triple the primary crystallization half-time[2].

Figure 5 shows a typical example of the plot of $\ln[1-I_{max}(t)/I_{max}(\infty)]$ against t for B5 crystallized at 28.7°C in the secondary crystallization (i.e. $0.95>I_{max}(t)/I_{max}(\infty)>0.6$). The plots for all PCL-*b*-PBs and PCL2 at every T_c could be sufficiently approximated by straight lines, and it was easy to evaluate K' from the slopes. This means that the secondary crystallizations for PCL-*b*-PB and PCL are phenomenologically approximated by equation (8).

Figure 6 shows the plots of θ against T_c for all the samples studied. The data points divide into two groups: θ for PCL2 and B4, where the microphase structure never appears before crystallization, is about 3.5 irrespective of T_c, while θ for B5, B6, B7 and B11, where a microphase structure certainly appears before crystallization, is around 2.2. The values of K and θ may be influenced by the variation of n through equation (3). This variation in n is, however, not responsible for the large difference in θ. *Figure 6* shows that the secondary crystallization of PCL-*b*-PB with a microphase structure becomes slower than that of PCL2 and B4 showing no microphase separation if the crystallization rate at the primary

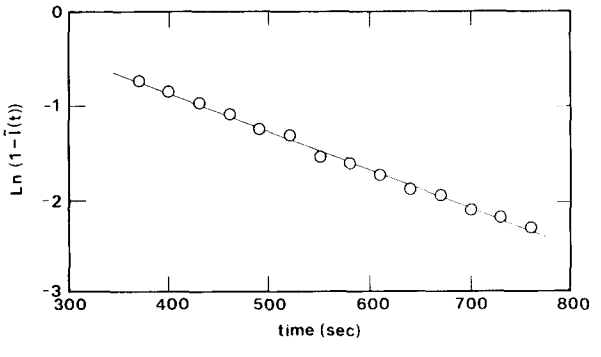

Figure 5 Plot of $\ln[1-I_{max}(t)/I_{max}(\infty)]$ against time for B5 crystallized at 28.7°C ($\tilde{I}(t)=I_{max}(t)/I_{max}(\infty)$)

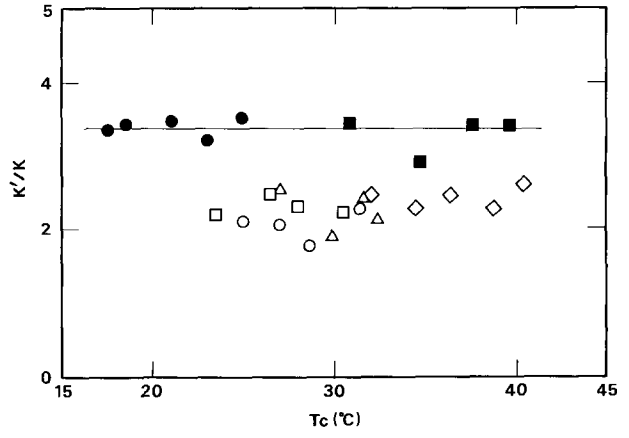

Figure 6 Plots of K'/K ($=\theta$) against crystallization temperature for B4 (●), B5 (○), B6 (□), B7 (◇), B11 (△) and PCL2 (■). The open symbols indicate that the system presents a microphase structure before crystallization

stage is the same (or K is the same). It is, however, impossible to detect any significant difference in θ among different microphase structures or molecular characteristics. *Figure 6* demonstrates that the crystallization rate of PCL-*b*-PB with a microphase structure is significantly retarded at the secondary crystallization. Therefore, the influence of the remaining microphase structure has to be taken into account to understand the crystallization behaviour of such block copolymers.

DISCUSSION

The crystallization behaviour of an ε-caprolactone–butadiene diblock copolymer (PCL-*b*-PB) was examined by synchrotron radiation small-angle X-ray scattering (SR-SAXS) and quantitatively analysed by methods widely used for homopolymer crystallization. The PCL-*b*-PB systems show a unique phase transformation according to the T_s, as shown in *Figure 1*. The molecular weights of our copolymers were sufficiently low such that freezing of the existing microphase structure, usually observed for high molecular weight copolymers[6–9], was mostly suppressed by the low viscosity of the system. As a result, dramatic changes in the SAXS curves could be observed.

The Avrami analysis of the primary crystallization did not show any significant difference between PCL-*b*-PB and a poly(ε-caprolactone) homopolymer (PCL2), suggesting that crystallization of the PCL block drives the primary crystallization without any influence from the existing microphase structure. In the secondary crystallization, on the other hand, the crystallization rate of PCL-*b*-PB with a microphase structure was significantly retarded compared with the case of PCL, indicating that the effect of the remaining microphase structure appears prominently at this stage.

The time-resolved SAXS curves have revealed that the increase in the crystalline morphology was accompanied by a decrease in the structure of the microphase at every moment of the phase transformation. This fact does not support the idea that the PCL block first crystallizes inside the PCL domain with the microphase structure unchanged, with further crystallization destroying the existing microphase structure, but indicates that the decay of the microphase structure occurs cooperatively with crystallization from the beginning of the phase transformation. Additionally, the sum of the scattered and diffracted intensities in normalized form was almost constant throughout the transition, suggesting that the microphase structure turns quickly into the crystalline morphology and no detectable third phase (for example, a disordered phase) appears during the phase transformation.

Mechanism of the phase transformation

The above experimental facts lead us to speculate about the phase transformation as follows. Here, we consider the case where a spherical microphase structure with the crystallizable block inside is replaced by a crystalline morphology, i.e. an alternating structure consisting of lamellae and amorphous layers. *Figure 7* illustrates two kinds of possible phase transformation. *Figure 7a* shows the case where the centre of mass of each sphere remains unchanged throughout the transformation and the crystallization begins within the sphere to deform the sphere through the formation of short lamellae. The amorphous block is rejected from the lamellae and simultaneously the neighbouring lamellae link together to develop into the crystalline morphology. In this mechanism, however, we cannot expect a large

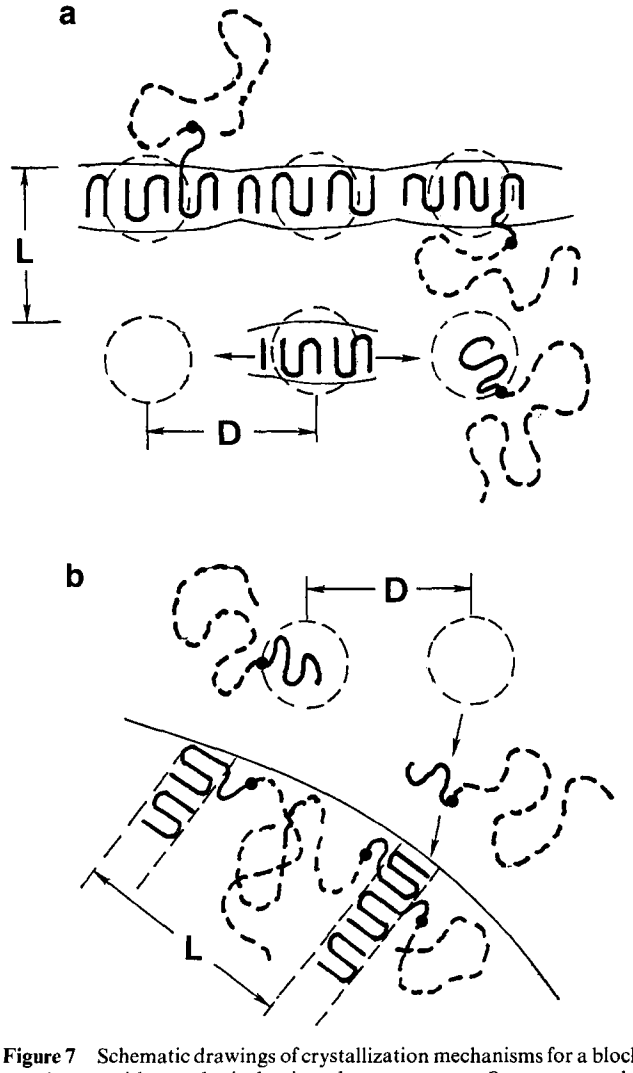

Figure 7 Schematic drawings of crystallization mechanisms for a block copolymer with a spherical microphase structure. D represents the characteristic length of the microphase structure and L is the alternating distance for the lamellae and amorphous layers after crystallization

shift in the repeat distance after crystallization, because the lamellae are substantially formed at the same position as the sphere to give a repeat distance that is unchanged. Even if the copolymer has a lamellar microphase structure before crystallization, this kind of phase transformation is unlikely because we have observed a large shift in the long spacing for B7 (with a lamellar microphase structure) after crystallization.

Figure 7b shows another phase transformation mechanism. Here, the crystal embryo appears independently of the existing microphase structure and it grows by absorbing molten block copolymers onto the growing surface to form the crystalline morphology. The molten block copolymer approaches the growing surface as a consequence of mutual diffusion through either of the following mechanisms: (1) a single block copolymer is pulled out from the sphere and reassociated with the crystalline morphology; or (2) the sphere itself coalesces with the crystalline morphology. Because the crystallization rate at the secondary stage is almost independent of the existing microphase structure, as shown in *Figure 6*, the growth mechanism should be the same irrespective of the microphase structure. Therefore, process (2) is unlikely, because the lamellar microphase structure cannot diffuse into the crystalline morphology as the sphere diffuses. It is concluded that the crystallization proceeds by a mechanism whereby the block copolymer is dissociated from the microphase structure and incorporated into the crystalline morphology. This mechanism also successfully explains the change in crystallization rate on going from the primary to the secondary stage, as discussed below.

Crystallization rate

In a compatible blend of crystalline and amorphous homopolymers, the amorphous component sometimes affects the crystallization rate. Wang and Nishi[44], for example, analysed the spherulitic growth rate for a binary blend of poly(vinylidene fluoride) and poly(methyl methacrylate) (PVF_2/PMMA) using the Lauritzen–Hoffmann equation. This equation consists of two terms: the free energy term required to form a critical nucleus from the melt and the mobility term associated with the transport of crystallizable segments through the melt. The large decrease in the spherulitic growth rate in the PVF_2/PMMA system was ascribed to a large variation in the glass transition temperature (or mobility term mentioned above).

Here, we try to explain qualitatively the crystallization rate of the present copolymers on the basis of a dissociation/association mechanism for the phase transformation discussed above. In general, an energy barrier (ΔE_1 in *Figure 8*) is known to exist in the nucleation step between molten polymers and perfect crystals. When this energy barrier is overcome (A→D→C), the following crystal growth progresses spontaneously if the mobility is large enough, as is the case with the present copolymers. For the microphase-separated block copolymers, the energy difference ΔE_2 between the homogeneous state (A) and the microphase structure (B) is not large, because our copolymers are of weak segregation judging from the absence of higher order diffractions in the SAXS curves, i.e. there are thick interfaces between the different domains. Therefore, microphase-separated copolymers crystallize by overcoming the energy barrier $\Delta E_1 + \Delta E_2$ ($\approx \Delta E_1$) through B→D→C in a similar fashion to the homopolymer which crystallizes through A→D→C, and no difference in the crystallization behaviour can be observed at the primary stage.

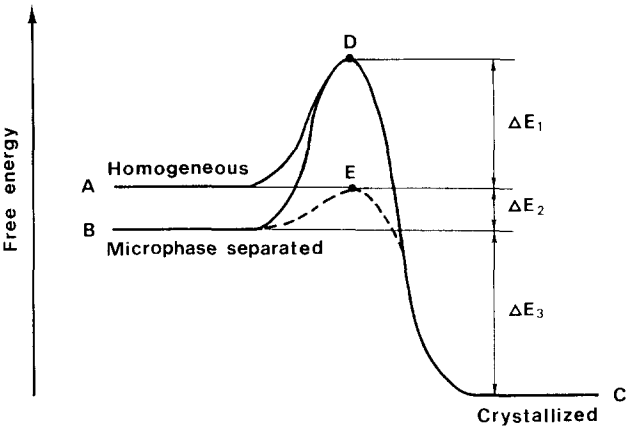

Figure 8 Free energy differences between the homogeneous state, the microphase structure and the crystalline morphology. ΔE_1 is the energy barrier between the homogeneous state and the crystalline morphology, and $\Delta E_1 + \Delta E_2$ is that between the microphase structure and the crystalline morphology

In the copolymer crystallization, the subsequent growth mechanism is quite different from that of the homopolymer. A small energy barrier ΔE_2 still remains between the microphase structure and the crystalline morphology. That is, when a block copolymer dissociates from the sphere to diffuse into the crystalline morphology (B→E→C), it causes an energy penalty through unfavourable interactions ΔE_2, and eventually the crystallization rate is retarded compared with the case of PCL2 and B4 without any microphase structure, where such an energy penalty is absent and crystal growth proceeds spontaneously. The process B→E→C occurs quickly when thermal energy overcomes ΔE_2, so that a third state cannot be detected by the SR-SAXS measurements. This situation is similar to the case of the growth of micelles consisting of amorphous–amorphous diblock copolymers in the presence of a good solvent, as discussed by Hashimoto *et al.*[45]. The energy barrier ΔE_2 becomes higher as the molecular weight of the copolymer increases and/or the interaction between the two blocks becomes unfavourable, and finally the structural rearrangement is practically impossible because of a high ΔE_2 between the two states. Freezing of the microphase structure, as observed by Cohen *et al.*[7] for a styrene–hydrogenated butadiene diblock copolymer with a high molecular weight, corresponds to an extremely high energy barrier between the microphase structure and the crystalline morphology.

The qualitative explanation of the mechanism of structural rearrangement mentioned above is plausible from the viewpoint of the crystallization rates at the primary and secondary stages. The explanation is also consistent with all the experimental results obtained in this study. A comprehensive study including the evaluation of the free energies ΔE_1, ΔE_2 and ΔE_3 in *Figure 8* is necessary for a quantitative discussion of the differences in crystallization behaviour between homopolymers and block copolymers. This study also elucidates the detailed mechanism of the phase transformation in microphase-separated copolymers.

ACKNOWLEDGEMENTS

We thank the staff of the Workshop for Experimentation and Practice, School of Engineering, Nagoya University for making the vacuum line used to synthesize the copolymers for this study. This work was supported in part by a grant from the General Sekiyu Research & Development Encouragement & Assistance Foundation, and has been performed under the approval of the Photon Factory Program Advisory Committee (proposal 91-245).

REFERENCES

1 Mandelkern, L. 'Crystallization of Polymers', McGraw-Hill, New York, 1964
2 Wunderlich, B. 'Macromolecular Physics 2', Academic Press, New York, 1976
3 Hirata, E., Ijitsu, T., Soen, T., Hashimoto, T. and Kawai, H. *Polymer* 1975, **16**, 249
4 Gervais, M. and Gallot, B. *Polymer* 1981, **22**, 1129
5 Zemel, I. S., Corrigan. J. P. and Woodward, A. E. *J. Polym. Sci. B* 1989, **27**, 2479
6 Seguela, R. and Prud'homme, J. *Polymer* 1989, **30**, 1446
7 Cohen, R. E., Cheng, P. L., Douzinas, K., Kofinas, P. and Berney, C. V. *Macromolecules* 1990, **23**, 324
8 Veith, C. A., Cohen, R. E. and Argon, A. S. *Polymer* 1991, **32**, 1545
9 Douzinas, K. C., Cohen, R. E. and Halasa, A. F. *Macromolecules* 1991, **24**, 4457
10 Ishikawa, S., Ishizu, K. and Fukutomi, T. *Polym. Commun.* 1991, **32**, 374
11 Li, W. and Huang, B. *J. Polym. Sci. B* 1992, **30**, 727
12 Yao, N., Li, X., Li, Y. and Nu. X. *Eur. Polym. J.* 1992, **28**, 831
13 Douzinas, K. C. and Cohen, R. E. *Macromolecules* 1992, **25**, 5030
14 Unger, R., Beyer, D. and Donth, E. *Polymer* 1991, **32**, 3305
15 Gast, A. P., Vinson, P. K. and Cogan-Farinas, K. A. *Macromolecules* 1993, **26**, 1774
16 Rangarajan, P., Register, R. A. and Fetters, L. J. *Macromolecules* 1993, **26**, 4640
17 Nojima, S., Kato, K., Yamamoto, S. and Ashida, T. *Macromolecules* 1992, **25**, 2237
18 Nojima, S., Nakano, H. and Ashida, T. *Polym. Commun.* 1993, **34**, 4168
19 Ito, K. and Yamashita, Y. *Macromolecules* 1978, **11**, 68
20 Santee Jr, E. R., Chang, R. and Morton, M. *J. Polym. Sci., Polym. Lett. Edn* 1973, **11**, 449
21 Rigby, D. and Roe, R. J. *Macromolecules* 1986, **19**, 721
22 Crescenzi, V., Manzini, G., Calzolari, G. and Borri, C. *Eur. Polym. J.* 1972, **8**, 449
23 Hashimoto, T., Shibayama, M. and Kawai, H. *Macromolecules* 1980, **13**, 1237
24 Elsner, G., Riekel, C. and Zachmann, H. G. *Adv. Polym. Sci.* 1985, **67**, 1
25 Gehrke, R. *Top. Curr. Chem.* 1989, **171**, 111
26 Nojima, S., Tsutsui, H., Urushihara, M., Kosaka, W., Kato, N. and Ashida, T. *Polym. J.* 1986, **18**, 451
27 Ueki, T., Kataoka, M., Inoko, Y., Amemiya, Y., Izumi, Y., Tagawa, H. and Muroga, Y. *Biophys. Chem.* 1985, **23**, 115
28 Nojima, S., Kato, K., Ono, M. and Ashida, T. *Macromolecules* 1992, **25**, 1922
29 Avrami, M. *J. Chem. Phys.* 1939, **7**, 1103
30 Avrami, M. *J. Chem. Phys.* 1940, **8**, 212
31 Avrami, M. *J. Chem. Phys.* 1941, **9**, 177
32 Wang, J., Alvarez, M., Zhang, W., Wu, Z., Li, Y. and Chu, B. *Macromolecules* 1992, **25**, 6943
33 Gehrke, R., Riekel, C. and Zachmann, H. G. *Polymer* 1989, **30**, 1582
34 Hillier, I. H. *J. Polym. Sci. A* 1965, **3**, 3067
35 Hoshino, S., Meinecke, E., Powers, J. and Stein, R. S. *J. Polym. Sci. A* 1965, **3**, 3041
36 Price, F. P. *J. Polym. Sci. A* 1965, **3**, 3079
37 Booth, A. and Hay, J. N. *Polymer* 1971, **12**, 365
38 Hoffman, D. M. and McKinley, B. M. *Polym. Eng. Sci.* 1985, **25**, 562
39 Godovsky, Y. K., Slonimsky, G. L. and Garbar, N. M. *J. Polym. Sci. C* 1972, **38**, 1
40 Ong, C. J. and Price, F. P. *J. Polym. Sci., Polym. Symp. Edn* 1978, **63**, 59
41 Nojima, S., Wang, D. and Ashida, T. *Polym. J.* 1991, **23**, 1473
42 Keith, H. D., Padden, F. J. and Russell, T. P. *Macromolecules* 1989, **22**, 666
43 Stein, R. S., Khambatta, F. B., Warner, F. P., Russell, T. P., Escala, A. and Balizer, E. *J. Polym. Sci., Polym. Symp. Edn* 1978, **63**, 313
44 Wang, T. T. and Nishi, T. *Macromolecules* 1977, **10**, 421
45 Mori, K., Hasegawa, H. and Hashimoto, T. *Polymer* 1990, **31**, 2368